High Resolution Upwind-Mixed Finite Element Methods for Advection-Diffusion Equations with Variable Time-Stepping

Clint N. Dawson

June, 1994

TR94-23

High Resolution Upwind-Mixed Finite Element Methods for Advection-Diffusion Equations with Variable Time-Stepping

Clint Dawson *

June 15, 1994

Abstract

Numerical methods for advection-diffusion equations are discussed based on approximating advection using a high-resolution upwind finite difference method, and incorporating diffusion using a mixed finite element method. In this approach, advection is approximated explicitly and diffusion implicitly. We first describe the basic procedure where each advection time-step is followed by a diffusion step. Because the explicit nature of the advective scheme requires a CFL time-step constraint, the basic procedure may be expensive, especially if the CFL constraint is severe. Two alternative time-stepping approaches are presented for improving computational efficiency while preserving accuracy. In the first approach, several advective time-steps are computed before taking a diffusion step. In the second approach, the advective time-steps are also allowed to vary spatially. Numerical results for these three procedures for a model problem arising in flow through porous media are given.

Keywords: Advection, diffusion, upwinding, mixed finite elements

1 Introduction

Explicit, upwind finite difference schemes based on slope-limiting [28] or flux-limiting [6] have become very popular over the last few years for solving linear and nonlinear advection equations. These schemes are so-called "high-resolution" [21] extensions of earlier methods developed by Godunov [17], Lax and Friedrichs [20], and others and combine numerical stability with second-order accuracy away from discontinuities in the solution. These schemes have the advantages that they are explicit in time and thus easy to implement, approximate shocks or sharp fronts accurately and with no oscillations, and are globally mass conservative. Because they were developed

*Dept. of Computational and Applied Mathematics, Rice University, Houston, TX 77251. This work was supported in part by grants from the Unites States Department of Energy.

for advection equations, they are also useful in designing methods for advection-dominated diffusion equations, where the diffusive flux is "small" relative to the advective flux. For these equations, operator-splitting can be used, where advection is first approximated using any of the above-mentioned finite difference schemes, then diffusion is incorporated using finite elements or finite differences, see, for example [9, 10].

The original development of slope- and flux-limiting methods was in one space dimension. Over the past several years, multidimensional extensions of these algorithms have been developed; see, for example, [5, 8, 30, 29]. Based on the work in [5, 11, 10], we have developed algorithms in two and three dimensions combining a slope-limiting approach for advection with a mixed finite element method for diffusion, the so-called "Godunov-Mixed Method" or GMM. This scheme has been implemented and applied to contaminant transport problems [7], and has been used to study the effects of nonlinear adsorption [16, 12, 18, 13, 15, 14]. The scheme has also been applied to the saturation equation which arises in modeling two-phase flow using the fractional flow formulation [14].

The GMM falls into a general class of methods we refer to as "Upwind-Mixed Methods" (UMM) where the advective flux is approximated using some type of upwinding technique, and diffusion is incorporated using a mixed finite element method. In this paper, we will outline the UMM and describe in some detail our implementation of the GMM. Though we will restrict attention to rectangular regions in $\mathbb{R}^2$, the scheme has been extended to $\mathbb{R}^3$ and can be extended to more general geometries using smooth mappings as described in [3]. We comment on these extensions toward the end of the paper.

In the UMM, the diffusion step involves solving a global system of equations, since diffusion is incorporated implicitly. Moreover, the advection step requires a CFL time-step constraint for stability. Thus, in a straightforward implementation of the UMM, where one advection step is followed by one diffusion step, a global system of equations must be solved every CFL time-step. In this paper, we examine two approaches for reducing the cost of this type of procedure while maintaining accuracy by allowing for variable time-steps. In the first approach, we simply use different time steps for advection and diffusion, with the advective time-step smaller than the diffusive time-step. This approach was described and analyzed in [11], but no numerical results were given. In the second approach, we use variable time-steps within the advection procedure itself, by dividing the domain into "zones", and using different CFL time-steps within each zone. Diffusion is again incorporated implicitly, but the diffusive time-step does not vary spatially. The use of spatially variable time-steps for solving one-dimensional conservation laws was described in [22]; the methods used here are similar but are multidimensional and spatially higher-order accurate.

Let Ω represent a spatial domain in $\mathbb{R}^2$, and let $T > 0$. We consider the transport equation [4]:

$$(\phi c)_t + \nabla \cdot (\mathrm{u}c - D\nabla c) = q\tilde{c}, \quad \text{on } \Omega \times (0, T]. \tag{1}$$

Here c is the concentration of some component flowing through the medium, ϕ is

the porosity of the medium, $\mathbf{u} = (u, v)$ is the velocity of the fluid, $D = D(\mathbf{u})$ is the hydrodynamic diffusion/dispersion tensor, q is the flow rate at sources/sinks, and $\tilde{c}$ is the concentration at sources/sinks, which is specified if $q > 0$ and $\tilde{c} = c$ if $q < 0$. D generally has the form

$$D(\mathbf{u}) = \alpha_m I + \frac{\alpha_l}{|\mathbf{u}|} \begin{bmatrix} u^2 & uv \\ uv & v^2 \end{bmatrix} + \frac{\alpha_t}{|\mathbf{u}|} \begin{bmatrix} v^2 & -uv \\ -uv & u^2 \end{bmatrix}. \tag{2}$$

where α_m is the molecular diffusivity and α_l and α_t are longitudinal and transverse mixing lengths, respectively. Initially, c satisfies

$$c(x, y, 0) = c^0(x, y), \quad \text{on } \Omega. \tag{3}$$

On the boundary $\mathcal{S}_T \equiv \partial\Omega \times (0, T]$, we assume $\partial\Omega = \Gamma_1 \cup \Gamma_2$, where Γ_1 is an inflow boundary with

$$(\mathbf{u}c - D\nabla c) \cdot \eta = \mathbf{u}c_1 \cdot \eta, \quad \text{on } \Gamma_1 \times (0, T], \tag{4}$$

and Γ_2 is an outflow-noflow boundary, with

$$D\nabla c \cdot \eta = 0, \quad \text{on } \Gamma_2 \times (0, T]. \tag{5}$$

Here η is the outward normal to $\partial\Omega$ and c_1 is a specified function.

The velocity $\mathbf{u}$ in (3) is assumed to satisfy Darcy's Law

$$\mathbf{u} = -K\nabla h, \quad \text{on } \Omega, \tag{6}$$

and the incompressibility condition

$$\nabla \cdot \mathbf{u} = q. \tag{7}$$

In (6), K is the hydraulic conductivity of the medium, and h is the hydraulic head. In this paper, we will assume $\mathbf{u}$ is given; however, in most cases, $\mathbf{u}$ is approximated using finite elements or finite differences and this approximation is used in (1). While we have assumed here single-phase flow, the transport schemes described below can also be used in multiphase flow, if we use the flow and transport model discussed in [23]. Assuming simple phase equilibrium, this model leads to transport equations of the same form as (1).

In applications where q models point sources/sinks, such as when injection and production wells are present, the velocity $\mathbf{u}$ can vary greatly in magnitude. In particular $\mathbf{u}$ is large near the wells and drops sharply as the distance from the well increases. This is obvious from (7) since in this case, q is represented by a sum of Dirac delta functions centered at the well locations. The CFL constraint necessary to guarantee stability of the advective finite difference scheme is

$$\max\left\{\frac{|u|\Delta t_A}{\phi h^x}, \frac{|v|\Delta t_A}{\phi h^y}\right\} \leq 1, \tag{8}$$

where Δt_A is the advective time-step, and h^x and h^y are mesh-spacings in the x and y directions, respectively. When $\mathbf{u}$ varies spatially, (8) can impose an unnecessarily severe restriction on the time-step in large parts of the domain. Thus, the second variable time-stepping approach we will discuss, where Δt_A varies spatially, is particularly useful for this case.

The paper is outlined as follows. In the next section, we give notation and describe three time-stepping methods. In Section 3, numerical results are given, with particular emphasis on cases where point sources/sinks are present. Extensions to three dimensions and general geometry are discussed in Section 4.

2 Description of Methods

Assume $\Omega = [0, L_x] \times [0, L_y]$, and partition Ω into rectangles $B_{ij} = [x_{i-1/2}, x_{i+1/2}] \times [y_{j-1/2}, y_{j+1/2}]$, $i = 1, \ldots, N_x$, $j = 1, \ldots, N_y$. Let $h_i^x = x_{i+1/2} - x_{i-1/2}$, $h_j^y = y_{j+1/2} - y_{j-1/2}$, and $h = \min_{i,j}(h_i^x, h_j^y)$. Let (x_i, y_j) denote the midpoint of B_{ij}.

Let $\Delta t_A > 0$ denote the advective time-step, and $\Delta t_D > 0$ denote the diffusive time-step. Let $t^n = n\Delta t_D$, $n = 0, 1, \ldots$. For any $r = r(x, y, t)$, let $r_{i,j}^n = r(x_i, y_j, t^n)$,

$$\partial_t r^n = (r^n - r^{n-1})/\Delta t_D,$$

and

$$r^{n-\theta} = (1 - \theta)r^n + \theta r^{n-1}, \quad 0 \le \theta \le 1. \tag{9}$$

Let $\tilde{\mathbf{z}}$ be given by

$$\tilde{\mathbf{z}} = -\nabla c, \tag{10}$$

and denote the diffusive flux by

$$\mathbf{z} = D\tilde{\mathbf{z}}. \tag{11}$$

Then, multiplying (1), (10), and (11) by test functions, integrating, and integrating (10) by parts we find

$$((\phi c)_t + \nabla \cdot (\mathbf{u}c + \mathbf{z}), w) = (q\tilde{c}, w), \quad w \in L^2(\Omega), \tag{12}$$

$$(\tilde{\mathbf{z}}, \mathbf{v}) = (c, \nabla \cdot \mathbf{v}), \quad \mathbf{v} \in H^0(\Omega; \mathrm{div}), \tag{13}$$

and

$$(\mathbf{z}, \tilde{\mathbf{v}}) = (D\tilde{\mathbf{z}}, \tilde{\mathbf{v}}), \quad \tilde{\mathbf{v}} \in H(\Omega; \mathrm{div}), \tag{14}$$

where

$$H(\Omega; \mathrm{div}) = \{\mathbf{v} = (v_1(x, y), v_2(x, y)) : v_1, v_2, \nabla \cdot \mathbf{v} \in L^2(\Omega)\},$$

and

$$H^0(\Omega;\mathrm{div}) = H(\Omega;\mathrm{div}) \cap \{\mathbf{v} : \mathbf{v}\cdot\eta = 0\}.$$

We employ this version of the mixed finite element method over the standard mixed method approach described in [10] because it allows for an easier implementation when D is a matrix [2].

Let $W_h \subset L^2(\Omega)$, $\mathbf{V}_h \subset H(\Omega;\mathrm{div})$, and $\mathbf{V}_h^0 \subset H^0(\Omega;\mathrm{div})$ denote the lowest-order Raviart-Thomas approximating spaces [24] defined on the partition of grid blocks $\{B_{ij}\}$. Here W_h consists of scalar functions w which are piecewise constant, while $\mathbf{V}_h$ consists of vector functions $\mathbf{v} = (v_1, v_2)$, where v_1 is a continuous, piecewise linear function in x and piecewise constant in y, and v_2 is piecewise constant in x and continuous, piecewise linear in y. A basis function corresponding to the first component of $\mathbf{v}$ is

$$\psi_{i+1/2,j}(x,y) = \begin{cases} \frac{x-x_{i-1/2}}{x_{i+1/2}-x_{i-1/2}}, & x_{i-1/2} \le x \le x_{i+1/2},\ \ y_{j-1/2} \le y \le y_{j+1/2}, \\ \frac{x_{i+3/2}-x}{x_{i+3/2}-x_{i+1/2}}, & x_{i+1/2} \le x \le x_{i+3/2},\ \ y_{j-1/2} \le y \le y_{j+1/2}, \\ 0, & \text{otherwise}, \end{cases} \tag{15}$$

for $1 \le i \le N_x - 1$, with the appropriate modifications for $i = 0$ and $i = N_x$. Thus, for any $\mathbf{v} = (v_1, v_2) \in \mathbf{V}_h$, v_1 can be written as

$$v_1(x,y) = \sum_{i=0}^{N_x}\sum_{j=1}^{N_y} v_1(x_{i+1/2}, y_j)\psi_{i+1/2,j}(x,y); \tag{16}$$

that is, v_1 is determined by its values at the points $(x_{i+1/2}, y_j)$. Similarly, v_2 is determined at $(x_i, y_{j+1/2})$.

In the UMM described below, we approximate c^n by $C^n \in W_h$, $\tilde{\mathbf{z}}^n$ by $\tilde{\mathbf{Z}}^n \in \mathbf{V}_h$, $\mathbf{z}^n$ by $\mathbf{Z}^n \in \mathbf{V}_h^0$, and $\mathbf{u}c^n$ by $\mathbf{F}^n = (f^n, g^n) \in \mathbf{V}_h$.

We now outline the UMM along with several time-stepping schemes.n

Time-stepping scheme I: $\Delta t_A = \Delta t_D$. We first consider the basic case where advection and diffusion are approximated with the same time step. Let $C^0 \in W_h$ be defined by

$$(\phi^0 C^0, w) = (\phi^0 c^0, w), \quad w \in W_h, \tag{17}$$

and for $n = 1, 2, \ldots$,

$$(\partial_t(\phi C)^n + \nabla\cdot(\mathbf{F}^{n-1} + \mathbf{Z}^{n-\theta}), w) = (q\tilde{C}^{n-\theta}, w), \quad w \in W_h, \tag{18}$$

$$(\tilde{\mathbf{Z}}^{n-\theta}, \mathbf{v}) = (C^{n-\theta}, \nabla\cdot\mathbf{v}), \quad \mathbf{v} \in \mathbf{V}_h^0, \tag{19}$$

$$(\mathbf{Z}^{n-\theta}, \tilde{\mathbf{v}}) = (D\tilde{\mathbf{Z}}^{n-\theta}, \tilde{\mathbf{v}}), \quad \tilde{\mathbf{v}} \in \mathbf{V}_h. \tag{20}$$

We will consider two choices of θ, $\theta = 0$ and $\theta = 1/2$. The first choice of θ gives a scheme which is first order in time, while $\theta = 1/2$ gives a scheme which is second order in time [10].

We note that setting $w = 1$ on B_{ij} and 0 elsewhere, the divergence theorem and $\mathbf{F}^{n-1} \in \mathbf{V}_h$ implies

$$(\nabla \cdot \mathbf{F}^{n-1}, w) = h_j^y [f_{i+1/2,j}^{n-1} - f_{i-1/2,j}^{n-1}] + h_i^x [g_{i,j+1/2}^{n-1} - g_{i,j-1/2}^{n-1}]. \tag{21}$$

In (18)-(20), C^n, $\tilde{\mathbf{Z}}^n$, and $\mathbf{Z}^n$ are calculated implicitly, by solving a linear algebraic system of equations, while $\mathbf{F}^{n-1}$ is calculated explicitly from the solution C^{n-1}. More will be said about $\mathbf{F}$ later. The system arising from (18)-(20) can be reduced to a symmetric, positive definite linear algebraic system in C^n only. Using the tensor product trapezoidal rule to approximate the integral on the left side of (19) and the two integrals in (20) gives a finite difference method in C^n, with a nine point stencil in two dimensions and a nineteen point stencil in three dimensions [2]. If D is a scalar quantity, then the stencil can be reduced to five points in two-dimensions and seven points in three dimensions. For example, assuming $\alpha_l = \alpha_t = 0$, ϕ constant, $\theta = 0$, and $h_i^x = h_j^y = h$, (18)-(20) can be reduced to the finite difference scheme

$$\begin{aligned} &\phi \frac{C_{ij}^n - C_{ij}^{n-1}}{\Delta t_D} + \frac{f_{i+1/2,j}^{n-1} - f_{i-1/2,j}^{n-1}}{h} + \frac{g_{i,j+1/2}^{n-1} - g_{i,j-1/2}^{n-1}}{h} \\ &\quad - \frac{\alpha_m}{h^2} \left[C_{i+1,j}^n + C_{i-1,j}^n - 4C_{i,j}^n + C_{i,j+1}^n + C_{i,j-1}^n \right] = q\tilde{C}_{ij}^n. \end{aligned} \tag{22}$$

for $i = 2, \ldots, N_x - 1$, $j = 2, \ldots, N_y - 1$, where $\tilde{C}_{ij}^n = \tilde{c}_{ij}^n$ if $q > 0$ and $\tilde{C}_{ij}^n = C_{ij}^n$ if $q < 0$. This formula can be extended to hold for all $1 \le i \le N_x$ and $1 \le j \le N_y$ by reflecting C across the boundary; i.e., setting $C_{0,j} = C_{1,j}$, etc.

Consider the advective flux across the $i + 1/2, j$ edge of B_{ij}. The edge $i, j + 1/2$ is analogous. The term $f_{i+1/2,j}^{n-1}$ approximates the advective flux through the $i + 1/2, j$ edge over the time interval $[t^{n-1}, t^n]$; that is,

$$f_{i+1/2,j}^{n-1} \approx \frac{1}{\Delta t_A h_j^y} \int_{t^{n-1}}^{t^n} \int_{y_{j-1/2}}^{y_{j+1/2}} (uc)(x_{i+1/2}, y, t) dy dt. \tag{23}$$

When the $i + 1/2, j$ edge of B_{ij} is on Γ_1, we set

$$f_{i+1/2,j}^{n-1} = \frac{1}{\Delta t_A h_j^y} \int_{t^{n-1}}^{t^n} \int_{y_{j-1/2}}^{y_{j+1/2}} (uc_1)(x_{i+1/2}, y, t) dy dt. \tag{24}$$

Hence, (24) along with the fact that the diffusive flux $\mathbf{Z}^{n-\theta}$ has zero normal component along the boundary, implies that the boundary conditions (4) and (5) are approximately satisfied.

At interior edges and on Γ_2, there are many ways that $f_{i+1/2,j}^{n-1}$ can be constructed. We base our scheme on the higher-order Godunov approach to calculating f given in [5, 10]. This approach consists of the following steps:

[A1] A piecewise bilinear function $\bar{C}^{n-1}$ is constructed from C^{n-1} by calculating x, y, and xy slopes on each grid block and applying slope-limiting.

[A2] Left and right states at the interface $(x_{i+1/2}, y_j)$ are calculated using $\bar{C}^{n-1}$ and the diffusive flux $\mathbf{Z}$.

[A3] f is evaluated using upwinding based on the sign of the velocity u.

The step [A1] gives $\bar{C}^{n-1}$ with

$$\begin{aligned}\bar{C}^{n-1}(x,y) &= C_{ij}^{n-1} + (x-x_i)\delta_x C_{ij}^{n-1} + (y-y_j)\delta_y C_{ij}^{n-1} \\ &\quad + (x-x_i)(y-y_j)\delta_{xy} C_{ij}^{n-1}, \quad (x,y) \in B_{ij}. \end{aligned} \tag{25}$$

The x, y, and xy slopes in (25) are calculated by applying a post-processing scheme to C^{n-1}. The slopes are limited so that no new extrema are introduced into the solution. A multidimensional limiting scheme described in [5] is used. The slopes are calculated element-by-element and are not costly to compute.

Step [A2] is based on (23) and the midpoint rule of integration:

$$\begin{aligned} f_{i+1/2,j} &\approx \frac{1}{\Delta t_A h_j^y} \int_{t^{n-1}}^{t^n} \int_{y_{j-1/2}}^{y_{j+1/2}} (uc)(x_{i+1/2}, y, t)\, dy dt \\ &= (uc)(x_{i+1/2}, y_j, t^{n-1/2}) + \mathcal{O}(\Delta t_A^2 + h^2). \end{aligned} \tag{26}$$

In this step, approximations to $c_{i+1/2,j}^{n-1/2}$ from the left and right of the interface are computed. We denote these approximations as C_L and C_R, respectively. By Taylor series and (1)

$$\begin{aligned} c_{i+1/2,j}^{n-1/2} &\approx c_{ij}^{n-1} + \frac{\Delta t_A}{2}(c_t)_{ij}^{n-1} + \frac{h_i^x}{2}(c_x)_{ij}^{n-1} \\ &= c_{ij}^{n-1} + \frac{h_i^x}{2}(c_x)_{ij}^{n-1} \\ &\quad + \frac{\Delta t_A}{2\phi_{ij}^{n-1}} \left[q\tilde{c} - \phi_t c - u c_x - u_x c - (vc)_y - \nabla \cdot z \right], \end{aligned} \tag{27}$$

where everything in brackets on the right side of (27) is evaluated at (x_i, y_j, t^{n-1}). Emulating (27), we set

$$\begin{aligned} C_L &= C_{ij}^{n-1} + \frac{h_i^x}{2}\left(1 - \frac{u_{i+1/2,j}^{n-1}\Delta t_A}{h_i^x \phi_{ij}^{n-1}}\right)\delta_x C_{ij}^{n-1} + \frac{\Delta t_A}{2\phi_{ij}^{n-1}}(q_{ij}\tilde{C}_{ij}^{n-1} - (u_x C + \phi_t C)_{ij}^{n-1}) \\ &\quad - \frac{\Delta t_A}{2h_j^y \phi_{ij}^{n-1}}\left(\beta_{i,j+1/2}^{n-1} - \beta_{i,j-1/2}^{n-1}\right) - \theta\frac{\Delta t_A}{\phi_{ij}^{n-1}}(\nabla \cdot \mathbf{Z}^{n-3/2})_{ij}. \end{aligned} \tag{28}$$

In (28), $\beta \approx vc$, and to calculate $\beta_{i,j+1/2}^{n-1}$, set

$$C_B = C_{ij}^{n-1} + \frac{h_j^y}{2}\delta_y C_{ij}^{n-1}, \tag{29}$$

and

$$C_T = C_{i,j+1}^{n-1} - \frac{h_{j+1}^y}{2}\delta_y C_{i,j+1}^{n-1}. \tag{30}$$

Then

$$g^{n-1}_{i,j+1/2} = c^{n-1}_{i,j+1/2} \begin{cases} C_B, & \text{if } v^{n-1}_{i,j+1/2} > 0, \\ C_T, & \text{otherwise.} \end{cases} \tag{31}$$

When $\theta = 1/2$, (28) formally represents a $\mathcal{O}(h^2 + \Delta t_A^2)$ approximation to $c^{n-1/2}_{i+1/2,j}$; when $\theta = 0$, the error is $\mathcal{O}(\Delta t_A + h^2)$. These bounds correspond to the overall accuracy of the scheme (17)-(20) [10].

The right state C_R is calculated similarly, using a Taylor series expansion of $c(x_{i+1/2}, y_j, t^{n-1/2})$ about the point (x_{i+1}, y_j, t^{n-1}). Finally,

$$f^{n-1}_{i+1/2,j} = u^{n-1/2}_{i+1/2,j} \begin{cases} C_L, & \text{if } u^{n-1/2}_{i+1/2,j} > 0, \\ C_R, & \text{otherwise.} \end{cases} \tag{32}$$

The scheme described by (17)-(32) is conservative in the following sense. Setting $w \equiv 1$ in (18), applying (24), multiplying by Δt_D, summing on n, and applying (17), we find for any N,

$$\begin{aligned} \int_\Omega \phi^N C^N dxdy &= \int_\Omega \phi^0 c^0 dxdy + \sum_{n=1}^{N} \int_\Omega q\tilde{C}^{n-\theta} dxdy\Delta t_D \\ &\quad - \int_0^{t^N} \int_{\Gamma_1} (\mathbf{u}c_1 \cdot \eta) dsdt - \sum_{n=1}^{N} \int_{\Gamma_2} (\mathbf{F}^{n-1} \cdot \eta) ds\Delta t_D. \end{aligned} \tag{33}$$

The true solution satisfies

$$\begin{aligned} \int_\Omega \phi^N c^N dxdy &= \int_\Omega \phi^0 c^0 dxdy + \int_0^{t^N} \int_\Omega q\tilde{c} dxdydt \\ &\quad - \int_0^{t^N} \int_{\Gamma_1} (\mathbf{u}c_1 \cdot \eta) dsdt - \int_0^{t^N} \int_{\Gamma_2} (\mathbf{u}c \cdot \eta) dsdt. \end{aligned} \tag{34}$$

We now discuss two approaches where Δt_A and Δt_D differ. These schemes are inherently first-order in time but more computationally efficient than the scheme described above. Thus, we take $\theta = 0$ from now on.

Time-stepping scheme II: $K\Delta t_A = \Delta t_D$. Assume $K \geq 1$ is an integer and $C^{n-1} \in W_h$ has been computed. Let $t^{n-1,k} = t^{n-1} + k\Delta t_A$, $k = 0, \ldots, K$. Define $C^{n-1,k} \in W_h$ as follows. Set $C^{n-1,0} = C^{n-1}$. Then, repeat for $k = 1, \ldots K$:

[B1] Given $C^{n-1,k-1}$, calculate advective fluxes $f^{n-1,k-1}_{i+1/2,j}$ and $g^{n-1,k-1}_{i,j+1/2}$ using the steps [A1]-[A3] above applied to $C^{n-1,k-1}$. From these values, one can construct $\mathbf{F}^{n-1,k-1} = (f^{n-1,k-1}, g^{n-1,k-1}) \in \mathbf{V}_h$.

[B2] Set

$$((\phi C)^{n-1,k}, w) = ((\phi C)^{n-1,k-1}, w) - \Delta t_A(\nabla \cdot \mathbf{F}^{n-1,k-1}, w), \quad w \in W_h. \tag{35}$$

To determine C^n, we use (18)-(20), with

$$\mathbf{F}^{n-1} = \frac{1}{K} \sum_{k=1}^{K} \mathbf{F}^{n-1,k-1}. \tag{36}$$

Time-stepping scheme III: spatially variable Δt_A. In this section we describe a scheme where Δt_A is allowed to vary spatially. As an example, consider dividing Ω into two zones Ω_1 and Ω_2 separated by an interface σ, where each zone consists of four grid blocks (see Figure 1). In general, we assume that the boundary between Ω_1 and Ω_2 is aligned with grid block boundaries in the partition $\{B_{ij}\}$. Let Δt_m denote the advective time step (satisfying a CFL constraint) in zone m, $m = 1$ or 2. Assume further that $\Delta t_2 = L\Delta t_1$, for some positive integer L, and $\Delta t_D = K\Delta t_2$ for some positive integer K.

Given $C^{n-1} \in W_h$, the advection step proceeds by first advecting the solution within Ω_1 for L steps up to time $t^{n-1} + \Delta t_2 \equiv t^{n-1,1}$. This procedure is defined for grid-blocks interior to Ω_1 following steps [B1]-[B2] and [A1]-[A3] above. At grid blocks which border Ω_2, the advective flux along the boundary σ is calculated as above, where the right state is evaluated using the current solution in Ω_2, namely C^{n-1}. At time $t^{n-1,1}$, we perform one advection step in Ω_2. Again, this is well-defined for interior grid blocks using [B1]-[B2] and [A1]-[A3] above. For those grid blocks in Ω_2 which border Ω_1, the flux on σ is constructed by enforcing continuity of flux across the boundary. More precisely, let $f_{i+1/2,j,R}$ denote the advective flux across σ as seen from Ω_2. Note that we have already calculated fluxes $f^{n-1,l}_{i+1/2,j}$, $l = 0, \ldots, L-1$ across σ in updating the solution in Ω_1. Thus, we set

$$f_{i+1/2,j,R} = \frac{1}{L} \sum_{l=0}^{L-1} f^{n-1,l}_{i+1/2,j}, \tag{37}$$

or, equivalently,

$$\Delta t_2 f_{i+1/2,j,R} = \sum_{l=0}^{L-1} \Delta t_1 f^{n-1,l}_{i+1/2,j}. \tag{38}$$

Once the solution is updated in Ω_2, we have taken one full advection step over the entire domain Ω. For $K > 1$, we repeat the procedure above K times until we reach time t^n, where diffusion is incorporated. Finally we obtain a new solution $C^n \in W_h$ and the whole process is repeated. Since the fluxes across σ match-up, this scheme is also conservative in the sense of (33).

Although we have only described this procedure using two zones, it is conceptually easy to generalize to more zones.

3 Numerical examples

In this section we present numerical results for the schemes described above. We consider (1)-(5) with $\Omega = [0, L] \times [0, L]$, $L = 25$ feet, $q = \bar{q}(\delta(0,0) - \delta(L,L))$ and

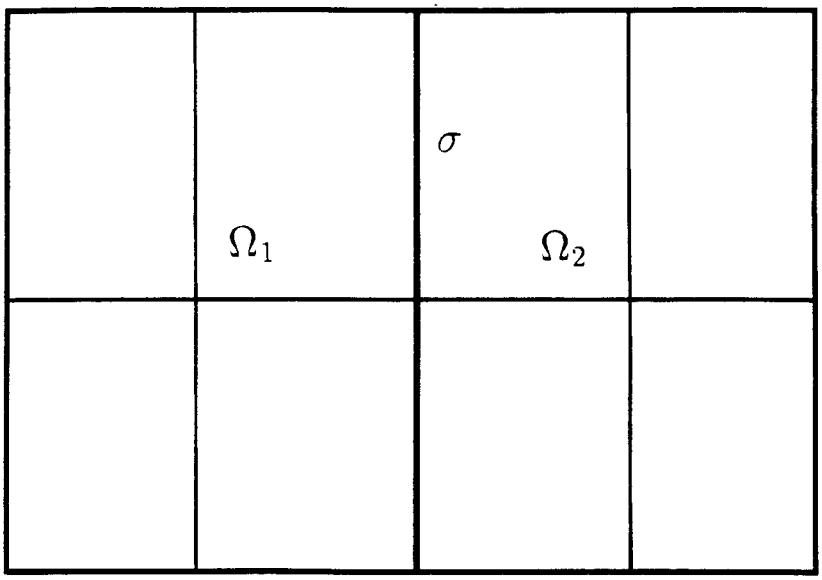

Figure 1: Division of Ω into two zones with different time steps

$\bar{q} = 1$ gallon/min, $\tilde{c} = 1$ at the injection well, $\phi \equiv 1$, $K = .000656$ feet/sec, $\partial\Omega = \Gamma_2$, and $c^0 \equiv 0$.

In all the runs below, $\theta = 0$, and in all contour plots of solutions, the contour levels are, from left to right, .96, .84, .72, .60, .48, .36, .24, and .12.

As a base case we take $\alpha_m = 0$, $\alpha_l = .3$ feet, and $\alpha_t = .03$ feet, and $\Delta t_A = \Delta t_D = \Delta t_{CFL}$, where Δt_{CFL} is the global CFL time step, defined by

$$\Delta t_{CFL} \max_{(x,y)\in\Omega} \left\{ \frac{|u(x,y)|}{h^x}, \frac{|v(x,y)|}{h^y} \right\} = 1.$$

We first solve for **u** using a block-centered finite difference approach, as described in [25]. The computational grid consists of 40x40 uniform grid blocks. In this case, $\Delta t_{CFL} = .002$ days. A contour plot of the numerical solution using time-stepping scheme I at $t = 1.2$ days is given in Figure 2. In Figure 3, a contour plot of the solution computed on an 80x80 uniform grid is given. Here $\Delta t_{CFL} = .0005$ days. Note that the solutions are very similar, thus the 40x40 solution is essentially converged.

Next we consider time-stepping scheme II outlined above, with $\Delta t_D = K\Delta t_A$. In Figure 4, a numerical solution at $t = 1.2$ computed on a 40x40 grid, with $\Delta t_D = .2$ days and $\Delta t_A = .002$ days, is given. Comparing Figures 2 and 4, the solutions are very similar, even though the physical diffusion in this problem is fairly significant. This figure demonstrates the accuracy of time-stepping scheme II, with $K = 100$.

In order to study time-stepping scheme III, with Δt_A spatially varying, we first take $\alpha_m = \alpha_l = \alpha_t = 0$; i.e., we consider advection only. In Figure 5, the numerical

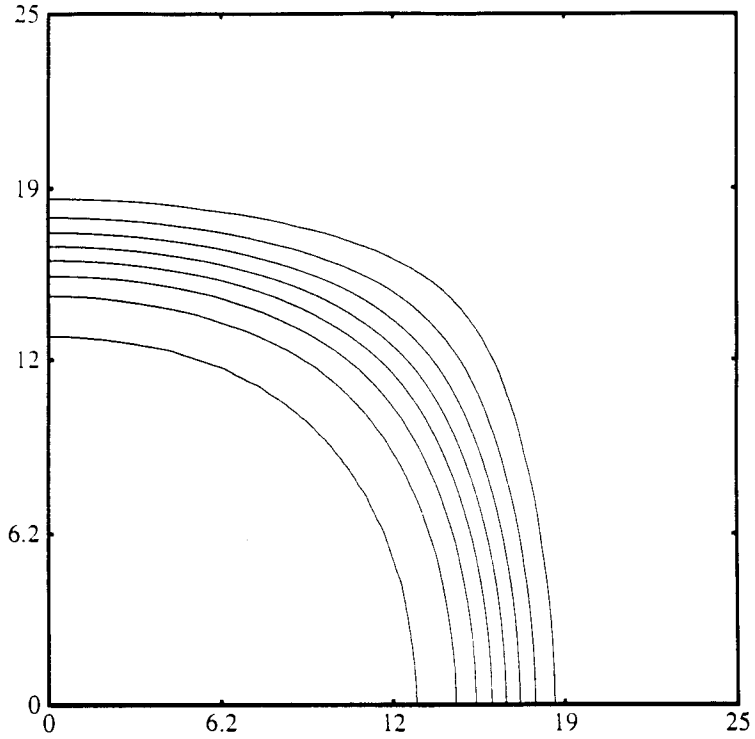

Figure 2: Base case: $C(x, y, t)$ at $t = 1.2$ days, 40x40 grid

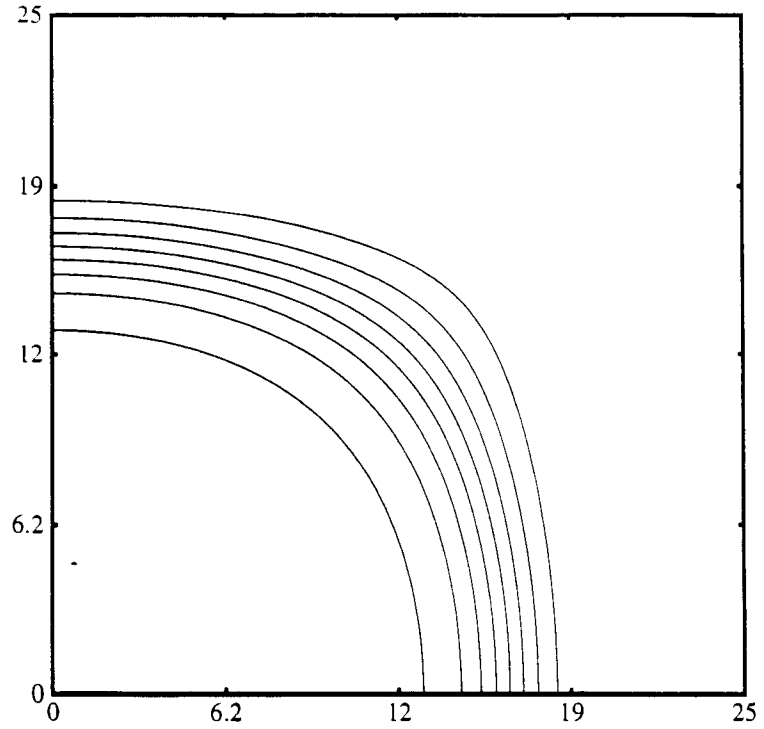

Figure 3: Base case: $C(x, y, t)$ at $t = 1.2$ days, 80x80 grid

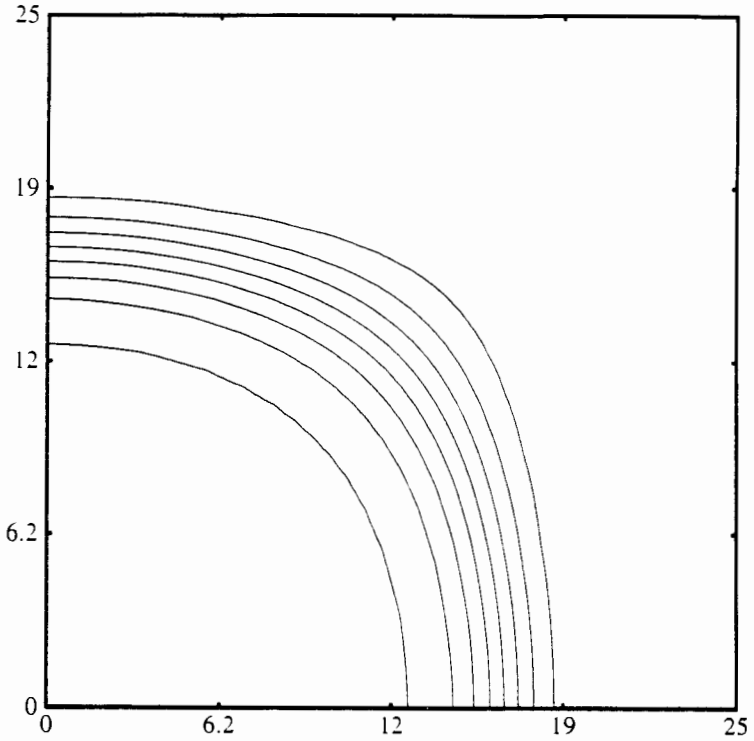

Figure 4: $\Delta t_D = 100\Delta t_A$: $C(x, y, t)$ at $t = 1.2$ days, 40x40 grid

solution on a 40x40 grid at $t = 1.2$ days with $\Delta t_A \equiv \Delta t_{CFL}$ is given. We now choose two time steps, $\Delta t_1 = \Delta t_{CFL}$ (=.002 days) and $\Delta t_2 = .05$ days, and divide Ω into two zones, Ω_1 and Ω_2, where Ω_1 consists of those cells where the cell CFL time-step is smaller than Δt_2, and Ω_2 contains the remaining cells. The cell CFL time-step is defined by

$$\Delta t_{i,j} = \min\left\{\frac{h_i^x}{|u_{i+1/2,j}|}, \frac{h_i^x}{|u_{i-1/2,j}|}, \frac{h_j^y}{|v_{i,j+1/2}|}, \frac{h_j^y}{|v_{i,j-1/2}|}\right\}.$$

In Ω_1, we set $\Delta t_A = \Delta t_1$, and in Ω_2, we set $\Delta t_A = \Delta t_2$. The regions Ω_1 and Ω_2 are shown in Figure 6. In this case, approximately 80% of the computational cells were located in Ω_2. The numerical solution for this case at $t = 1.2$ days is given in Figure 7. Note that this solution is very similar to the solution in Figure 5, with even slightly less numerical diffusion. This effect is due to the fact that the size of the numerical diffusion depends on how close Δt_A is to $\Delta t_{i,j}$. The closer these two quantities are, the less numerical diffusion inherent in the scheme. Thus, by allowing the time-step to be larger in parts of the domain, we have actually produced a more accurate answer.

In Figures 8 and 9, we repeat these calculations on an 80x80 grid. In the second case, $\Delta t_1 = \Delta t_{CFL} = .0005$ days, and $\Delta t_2 = .025$ days. Again, approximately 80% of the computational cells were located in Ω_2.

As a final example, we repeat the 40x40 calculation in Figure 7, adding diffusion.

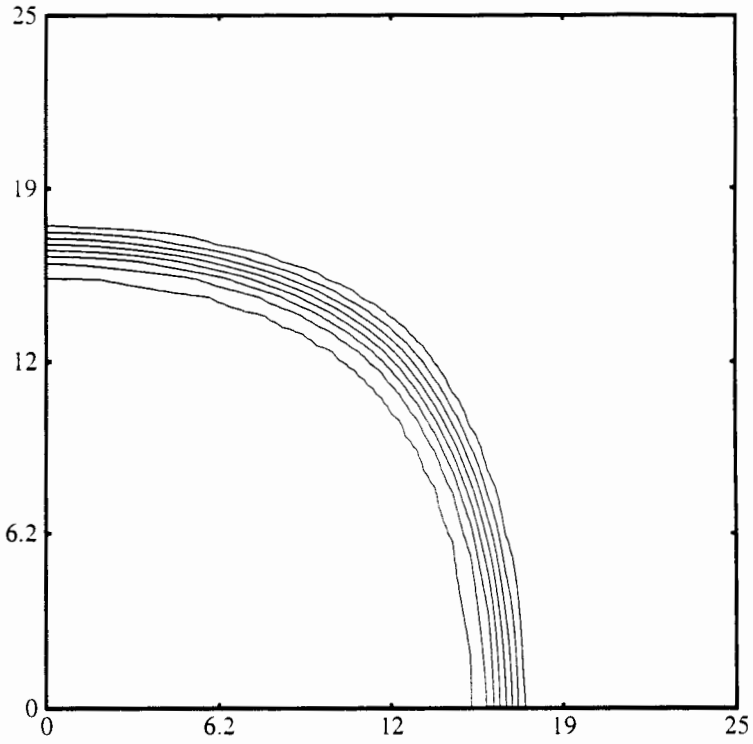

Figure 5: No diffusion, $\Delta t_A \equiv \Delta t_{CFL}$: $C(x, y, t)$ at $t = 1.2$ days, 40x40 grid

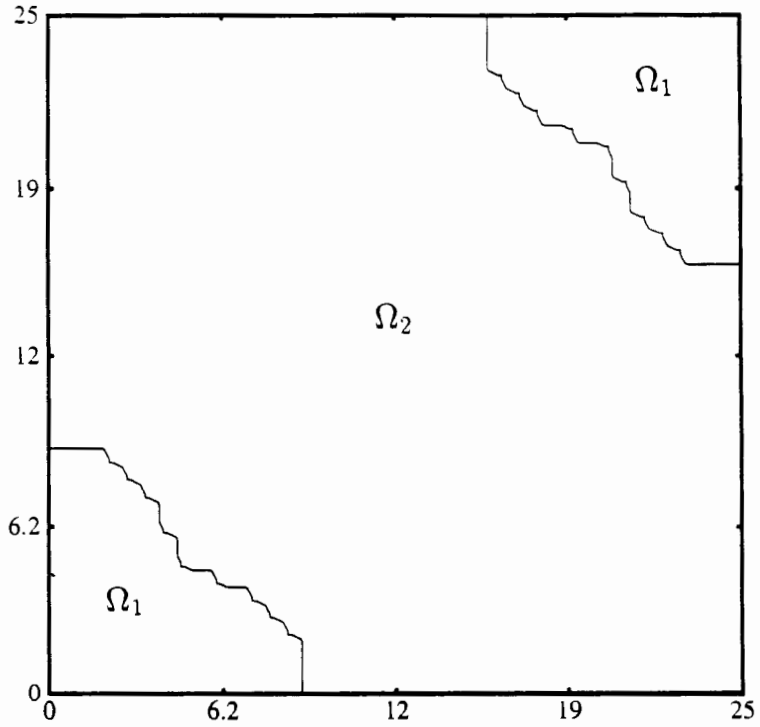

Figure 6: Regions Ω_1 and Ω_2 for spatially varying Δt_A case

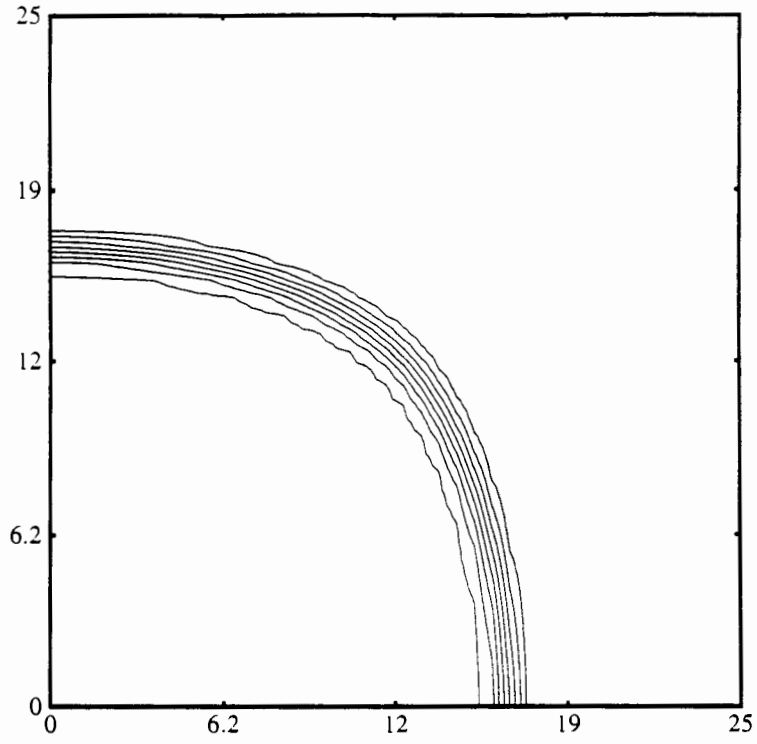

Figure 7: No diffusion, Δt_A spatially varying: $C(x, y, t)$ at $t = 1.2$ days, 40x40 grid

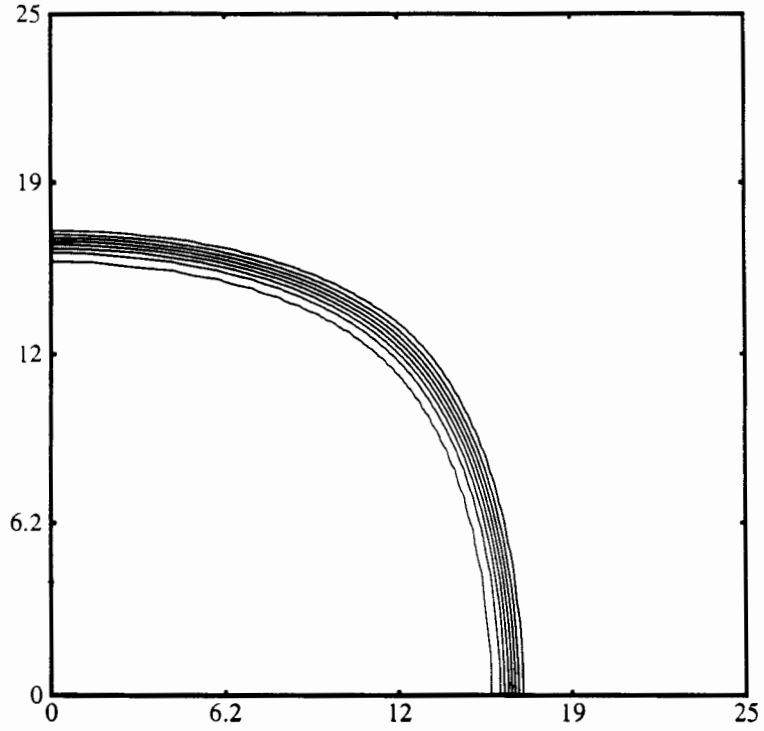

Figure 8: No diffusion, $\Delta t_A \equiv \Delta t_{CFL}$: $C(x, y, t)$ at $t = 1.2$ days, 80x80 grid

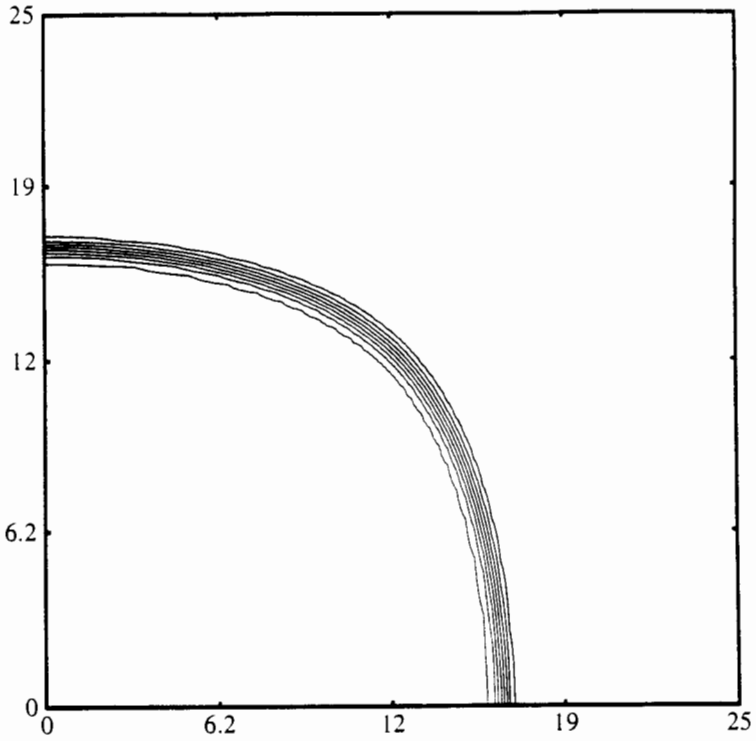

Figure 9: No diffusion, Δt_A spatially varying: $C(x, y, t)$ at $t = 1.2$ days, 80x80 grid

In this case, $\alpha_l = .3$ feet, $\alpha_t = .03$ feet, and $\Delta t_D = .05$ days. The solution is given in Figure 10. Note that this solution is virtually identical to the solutions given in Figures 2 and 4.

In all of the examples described here, the scheme conserved mass exactly, in the sense that for any time t^N,

$$\int_\Omega C^N dxdy = \sum_{n=1}^{N} \int_\Omega q\tilde{C}^n dxdy\Delta t_D. \tag{39}$$

4 Remarks on Extensions

The UMM extends easily to brick elements in three space dimensions. In this case, to construct the advective flux we first construct a piecewise trilinear function in each grid block by calculating x, y, z, xy, xz, and yz slopes, and applying slope-limiting. The analogous formulas to (28)-(31) for calculating the left and right states used to calculate the advective fluxes are again derived by Taylor expansion. In three dimensions, to calculate a left state to be used in constructing the x-flux at the point $(x_{i+1/2}, y_j, z_k)$, we expand c at the point $(x_{i+1/2}, y_j, z_k, t^{n-1/2})$ about the point (x_i, y_j, z_k, t^{n-1}). A formula similar to (28) is obtained with an additional flux difference in the z-direction, similar to the β term in (28).

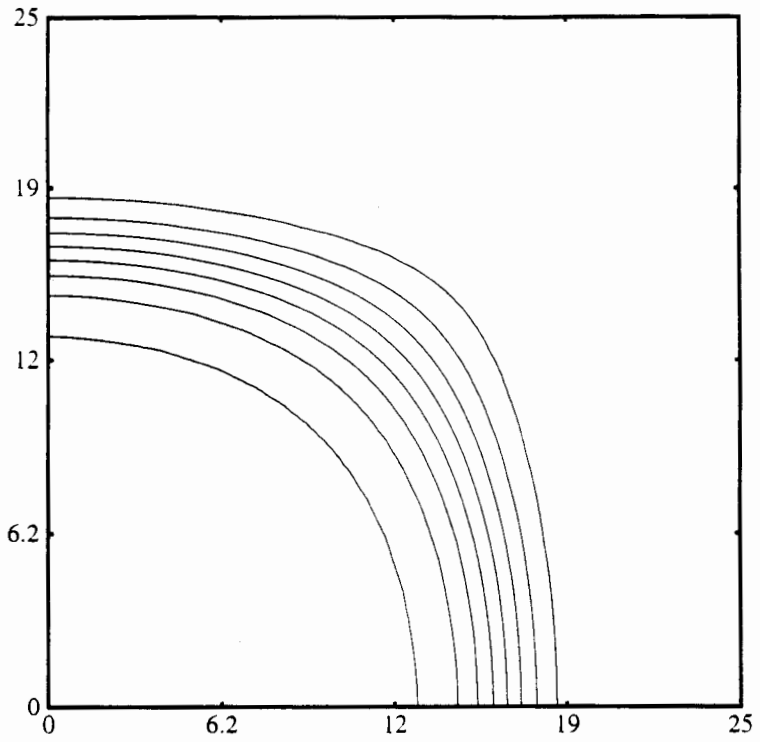

Figure 10: Δt_A spatially varying, $\Delta t_D = .05$ days: $C(x, y, t)$ at $t = 1.2$ days, 40x40 grid

The methods described here have all assumed a rectangular discretization. We can incorporate more general geometry into the method by using the techniques discussed in [3]. These techniques assume that the physical domain can be globally mapped to a rectangular computational domain using a $\mathcal{C}^2$ map. This does not impose a terribly severe restriction on the physical domain. There has been much effort in recent years in generating such maps for very complicated domains, see, for instance [27]. The vector quantities used in the method, namely, the diffusive and advective fluxes, and the velocity, are mapped using the Piola transformation [26, 3], which preserves normal fluxes. The bottom line is we end up solving a transformed equation of the same form as (1) on a rectangular domain, and mapping the solution back to the physical domain.

The UMM can also be extended to triangular and tetrahedral elements. There has been much work in recent years in extending the flux-limiting and slope-limiting methods to triangular elements (see, for example, [19]). These methods can be combined with efficient mixed methods for triangular elements as discussed in [1].

References

[1] T. Arbogast, C. N. Dawson, and P. T. Keenan, *Mixed finite elements as finite differences for elliptic equations on triangular meshes*, Technical Report TR93-57, Dept. of Comp. and Appl. Math., Rice University, 1993.

[2] T. Arbogast, M. F. Wheeler, and I. Yotov, *Mixed finite elements for elliptic problems with tensor coefficients as finite differences*, Technical Report TR94-02, Dept. of Comp. and Appl. Math., Rice University, 1994.

[3] T. Arbogast, M. F. Wheeler, and I. Yotov, *Mixed finite elements on general geometry*, in preparation.

[4] J. Bear, *Dynamics of fluids in porous media*, Elsevier, New York, 1972.

[5] J. B. Bell, C. N. Dawson, and G. Shubin, *An unsplit, higher-order Godunov method for scalar conservation laws in multiple dimensions*, J. Comput. Phys. **74**, pp. 1-24, 1988.

[6] J. P. Boris and D. L. Book, *Flux corrected transport I, SHASTA, a fluid transport algorithm that works*, J. Comput. Phys. **11**, pp. 38-69, 1973.

[7] C. Y. Chiang, G. Raven, and C. N. Dawson, *How to relate monitoring well and aquifer solute concentrations*, to appear in J. Groundwater.

[8] P. Colella, *Multidimensional upwind methods for hyperbolic conservation laws*, J. Comput. Phys. **87**, pp. 171-200, 1990.

[9] C. N. Dawson, *Godunov-mixed methods for advective flow problems in one space dimension*, SIAM J. Numer. Anal. **28**, pp. 1282-1309, 1991.

[10] C. N. Dawson, *Godunov-mixed methods for advection-diffusion equations in multidimensions*, SIAM J. Numer. Anal. **30**, pp. 1315-1332, 1993.

[11] C. N. Dawson, *Godunov-mixed methods for advection-diffusion equations*, Ph.D. Thesis, Dept. of Mathematical Sciences, Rice University, 1988.

[12] C. N. Dawson, *Simulation of nonlinear contaminant transport in groundwater by a higher order Godunov-mixed finite element method*, Applications of Supercomputers in Engineering II, C. A. Brebbia, D. Howard, and A. Peters, eds., Computational Mechanics Publications, Southamption, UK, pp. 419-433, 1991.

[13] C. N. Dawson, *Modeling of nonlinear adsorption in contaminant transport*, to appear in Proceedings, Computational Methods in Water Resources '94.

[14] C. N. Dawson, *Upwind-Mixed Methods for Contaminant Transport with Nonlinear, Nonequilibrium Adsorption Kinetics*, to appear in Proceedings, Workshop on Finite Element Methods in Environmental Applications, Austin, Texas, 1994.

[15] C. N. Dawson, C. J. van Duijn, and R. E. Grundy, *Large-time asymptotics in contaminant transport in porous media*, to appear.

[16] C. N. Dawson and M. F. Wheeler, *Characteristic methods for modeling nonlinear adsorption in contaminant transport*, Proceedings, 8th International Conference on Computational Methods in Water Resources, Venice, Italy, 1990, Computational Mechanics Publications, Southampton, U. K., pp. 305-314.

[17] S. K. Godunov, *A finite difference method for the numerical computation of discontinuoussolutions of the equations of fluid dynamics*, Mat. Sb. **47**, pp. 271-290, 1959 (Russian).

[18] R. E. Grundy, C. J. van Duijn, and C. N. Dawson, *Asymptotic profiles with finite mass in one-dimensional contaminant transport through porous media: the fast reaction case*, Quarterly Journal of Mechanics and Applied Mathematics, Vol. 47, Pt. 1, pp. 69-106, 1994.

[19] A. Harten and S. R. Chakravarthy, *Multi-dimensional ENO schemes for general geometries*, ICASE Report No. 91-76, 1991.

[20] P. D. Lax, *Shock waves and entropy*, in Contributions to Nonlinear Functional Analysis, E. H. Zarantonello, ed., Academic Press, New York, pp. 603-634, 1971.

[21] R. J. LeVesque, *Numerical methods for conservation laws*, Birkhäuser Verlag, Basel, 1990.

[22] S. Osher and R. Sanders, *Numerical approximations to nonlinear conservation laws with locally varying time and space grids*, Math. Comp. **41**, pp. 321-336, 1983.